Soil Dynamics and Earthquake Engineering 157 (2022) 107253

Contents lists available at ScienceDirect

Soil Dynamics and Earthquake Engineering

journal homepage: www.elsevier.com/locate/soildyn

Unbiased simplified seismic fragility estimation of non-ductile infilled RC structures

Al Mouayed Bellah Nafeh, Gerard J. O'Reilly *

Centre for Training and Research on Reduction of Seismic Risk (ROSE Centre), Scuola Universitaria Superiore IUSS Pavia, Palazzo del Broletto, Piazza della Vittoria 15, Pavia, 27100, Italy

ARTICLE INFO

Keywords:
Infilled frame
Seismic assessment
Collapse
Seismic risk
Performance

ABSTRACT

Infilled reinforced concrete (RC) buildings represent a prevalent taxonomy class in the Mediterranean region. Many were constructed before proper seismic provisions and detailing were enforced meaning they typically possess non-ductile failure mechanisms. Therefore, their simple but adequate seismic fragility estimation remains a challenge for the research community and practitioners. Moreover, their performance quantification can typically require characterisation via detailed numerical models that capture salient behaviour features, which involves extensive non-linear dynamic analyses with large computational burden. In this regard, an unbiased seismic fragility estimation methodology for the simplified assessment of infilled RC frame structures is described for both collapsing and non-collapsing scenarios. Its development is using extensive cloud analyses carried out with a large set of oscillators representative of the infilled RC frame's structural behaviour to permit the well-established pushover-based methods to be adopted in practice. The result is a novel set of empirical relationships relating the seismic behaviour of these typologies to their pushover curve parameters to allow practitioners to perform an accurate risk assessment and verification in an expedited manner. The choice of average spectral acceleration as the intensity measure used to characterise the fragility parameters for these relationships is shown to present notable advantages in reducing bias compared with other existing approaches. The results are validated via comparison with a detailed hazard-consistent assessment of case studies from a database of three-dimensional archetype building models. These were also developed here to capture the temporal evolution of building codes and architectural features of the building class in Italy.

1. Introduction

Reinforced concrete (RC) buildings with unreinforced masonry infill panels constitute a significant portion of the southern European building stock generally and the Italian built environment specifically. Buildings were typically designed to resist gravity loads only or were designed before the introduction of modern seismic design guidelines (i.e. capacity-based design). These are typically required to promote a ductile and stable mechanism by most modern-day design codes (e.g. Eurocode 8 (EC8) [1] and NTC18 [2]). Structural elements were designed considering allowable stress and constructed with smooth reinforcing bars, low compressive strength concrete, inadequate transverse detailing, and without any proper joint detailing. This resulted in many instances of brittle and non-ductile mechanisms forming, mainly in the columns and beam-column joints. Past earthquake reconnaissance observations [3] following the strong motion event of 2016 in Central Italy reported many occurrences of extensive damage and collapse cases in RC buildings with infills due to shear and flexural failure of structural members. Furthermore, infills were typically used in construction practice due to their beneficial thermal and acoustic insulation properties. However, these elements were not considered in the design process and their effect on the structural response was usually neglected. This has implications on the lateral-load bearing capacity of these buildings and the interaction between infill wall panels and the surrounding RC frame components. Sudden infill panel rupture causes differential stiffness between storeys which may lead to the occurrence of a soft-storey mechanism. The consequences of such were also reported after the 2009 earthquake in L'Aquila [4–6].

The assessment of seismic performance, within modern performance-based earthquake engineering (PBEE) [7], requires an adequate quantification of the exceedance of a structural performance level typically related to a structural demand level, quantified via an

* Corresponding author. ,
E-mail addresses: mouayed.nafeh@iusspavia.it (A.M.B. Nafeh), gerard.oreilly@iusspavia.it (G.J. O'Reilly).

https://doi.org/10.1016/j.soildyn.2022.107253
Received 1 January 2022; Received in revised form 21 February 2022; Accepted 11 March 2022
Available online 24 March 2022

engineering demand parameter (EDP). Fragility curves are typically used for this purpose as they represent the interface between the intensity of ground-shaking described by an intensity measure (IM) and the probability that a damage level, or EDP threshold, is exceeded. Fragility curves can be quantified empirically through experimental observation and data collection, expert judgement or analytically [8–10]. Analytical fragility functions require the numerical modelling of a case-study structure, ground-motion selection and extensive non-linear dynamic analyses. These elements of performance assessment can be demanding in terms of computational effort, specifically related to the time required for identifying suitable ground motion records and conducting non-linear dynamic analysis. To overcome this, simplified tools for the assessment of RC frame structures have provided an efficient alternative to implement in practice while offering a trade-off between simplicity and accuracy [11], with the introduction of the SPO2IDA [12], SPO2FRAG [13] and other simplified methodologies [14–19]. Amongst the methodologies mentioned, only the empirical relationships developed by Dolšek and Fajfar [14,15] apply to infilled RC structures to the authors' knowledge. However, their procedure was based on the spectral acceleration at the fundamental period of the structure, which has been shown to be a sub-optimal intensity measure for non-ductile infilled RC frame structures [20]. Moreover, their analysis used an equivalent SDOF model with infinite ductility capacity, meaning the median collapse intensity of the structural system is likely to be overestimated, as shown recently by Nafeh et al. [21]. These simplified approaches utilise the so-called R-μ-T relationships for a direct estimation of the seismic demand on the non-linear systems; R represents the strength ratio, or the strength reduction factor, relating the elastic spectral acceleration demand to the spectral acceleration which causes yielding of the structural system. In EC8, for example, it is encountered as part of the behaviour factor accounting for the deformation and energy dissipation capacity of the structural system; T is the initial period and μ denotes ductility demand. These tools subsequently aid users in the quantification and mitigation of seismic risk compatible with well-known guidelines [22,23]. For example, the inclusion of SPO2IDA within the FEMA P-58 guidelines [9] may be considered a testimony to the added value of such simplified tools.

However, tools such as SPO2IDA and other R-μ-T relationships typically utilise extensive results of incremental dynamic analyses (IDA) on single-degree-of-freedom (SDOF) systems for the quantification of seismic response and employ IMs that may be sub-optimal for certain structural systems, namely the spectral acceleration at first mode period, $Sa(T_1)$. Furthermore, studies [24,25] have highlighted the influence of amplitude scaling of records adopted in dynamic analysis procedures such as IDA on the response. Several past studies have also examined the suitability of IMs for different structural typologies to identify the advantages of each considering different scenarios. For example, O'Reilly [28] investigated potential IM choices for the seismic risk assessment of bridge portfolios, while Heresi et al. [27] addressed the benefits and drawbacks of several IMs in the regional assessment of low-rise wood framed structures. In subsequent sections, the impact of these choices is addressed in terms of bias on collapse estimation and a more suitable option for the simplified response estimation is explored.

To this end, the study proposes a simplified assessment tool based on empirical relationships using the pushover backbone response of a structure. The tool is tailored specifically for non-ductile infilled RC frame structures by employing a large set of representative SDOF systems. Moreover, the approach addresses the shortcomings of the choice of IM and dynamic procedures requiring amplitude scaling of records and the potentially biasing influence on the response. The empirical relationships derived and implemented in the simplified tool provided are further validated in terms of accurately quantifying collapse and non-collapse response predictions when compared with extensive dynamic analysis results. This comparison is performed using an *ad hoc* database of representative infilled RC typologies described in Appendix A and developed here. This database incorporates architectural features and geometrical layouts typical of these buildings, with different storey numbers, floor area, plan layout and other features considered.

The overall result is a simplified tool that can directly estimate the seismic fragility of non-ductile infilled RC frames with masonry infill using recent advances to avoid bias due to scaling and poor IM choice. This allows practitioners to assess these typologies in a more refined and expedited manner, whilst still fitting in with the risk-oriented goals of PBEE.

2. Potential bias

A performance-based assessment requires the quantification of structural (and non-structural) performance, typically requiring ground motion record selection and extensive non-linear dynamic analyses. There are alternative procedures available to characterise the relationship between the EDP and IM, namely: IDA [29], multiple stripe analysis (MSA) [30] and cloud analysis [31], for example. IDA performs several analyses by incrementally scaling a single set of records until the first trace of collapse is identified. MSA, however, utilises a hazard-consistent records at each intensity level corresponding to a single stripe. Cloud analysis, which does not require any direct scaling, utilises ground motions that satisfy some general criteria related to magnitude and distance bins, among other parameters.

Davalos and Miranda [36] examined the potential impacts of ground motion amplitude scaling and noted that existing literature provides contrasting conclusions; some studies [37–39] suggest minimal impact, whereas others [25,34,40–42] noted a significant influence. Based on their own study, Davalos and Miranda [36] concluded that record scaling leads to notable bias in quantifying deformation demands and collapse risk. Davalos and Miranda [24] also noted the role of IM in overestimating the probability of collapse due to higher scaling when using $Sa(T_1)$.

In recent years, various IMs have been investigated, such as filtered incremental velocity, *FIV3* [43], average spectral acceleration, Sa_{avg} [44], peak ground acceleration (PGA) [5,45], peak ground velocity (PGV) [46,47] and $Sa(T_1)$ [48]. A comparison of the performance of *FIV3*, Sa_{avg}, $Sa(T_1)$ and other relevant IMs like PGA specifically for the case of non-ductile infilled RC frames is reported in O'Reilly [20]. While *FIV3* remains promising for predicting the collapse performance, Sa_{avg} has established interest as a powerful performance predictor. The definition of Sa_{avg} inherently considers spectral acceleration values around the fundamental period, T_1. As such, period elongation effects of a structural system up to collapse, as well as contributions of higher modes at periods lower than T_1, are directly considered. O'Reilly [20] highlighted the unbiased prediction of Sa_{avg} to ground motion velocity-based characteristics when compared to $Sa(T_1)$, which is the IM that has been largely used to date in simplified methodologies. Kohrangi et al. [49] also noted lower dispersions associated with the ground motion prediction equations for the case of Sa_{avg}, implying higher predictability compared to a single $Sa(T)$. These reasons have contributed towards making Sa_{avg} a key IM for the reduction of uncertainty in risk-based analyses and point towards the need for its integration within simplified procedures following PBEE: a key focus of this work.

To illustrate this potential influence of scaling factors (SFs) and IM choice on non-linear demands, a simple assessment was conducted. A set of SDOFs previously analysed in Nafeh et al. [21] was used. IDA was conducted to collapse using the INNOSEIS European record sets [50] for medium and high seismicity. Results in terms of collapse intensity were extracted for low ($T < 0.2$s), moderate ($0.2\text{s} < T < 0.5$s) and high ($T > 0.5$s) periods of vibration and are presented in Fig. 1. Scaling bias was quantified using the intensity residual ε_i for each ground motion i, given by Equation (1).

$$\varepsilon_i = \frac{s_i}{\hat{s}} \tag{1}$$

where s_i and $\hat{s}$ are the collapse intensities of single records and the

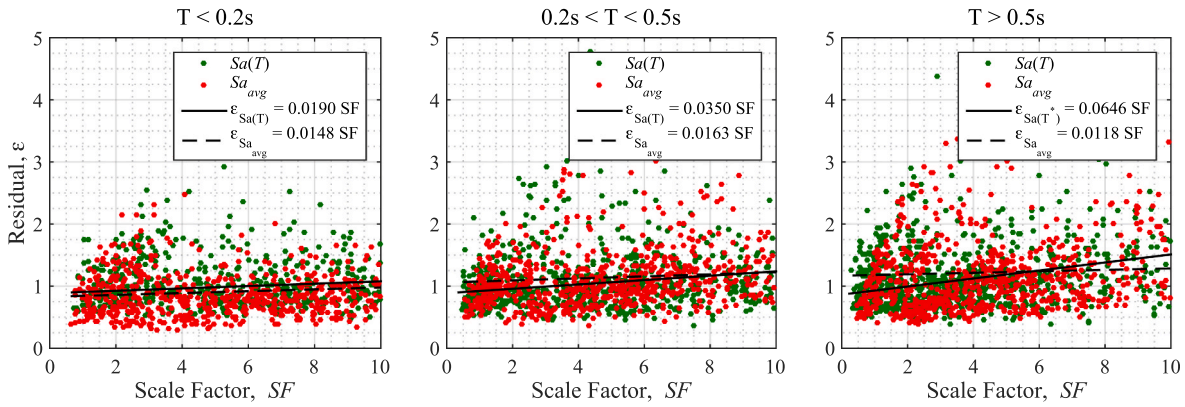

Fig. 1. Illustration of the trend between the residual, ε, and the ground motion scale factor, *SF*, required to induce collapse for SDOF systems with low, moderate and high periods of vibration obtained from IDA.

median collapse intensities for the studied SDOF system, respectively. A high residual indicates that a higher-than-average intensity was required for a certain record and vice-versa. The objective is to look for a trend between the residual and the scaling factors, which when compared in Fig. 1, the choice of IM was noted to exhibit a notable influence in addition to the period *T*. For example, when fitted with a simple linear regression, the difference in trend slopes was found to be trivial at short periods (0.0190 for $Sa(T)$ and 0.0148 for Sa_{avg}) suggesting a low influence of the record scaling in the prediction of the collapse intensities for these stiffer systems. However, this influence is evident for a higher *T*. The slope corresponding to the $Sa(T)$ cases increased notably, indicating that it becomes heavily impacted by the SF, while Sa_{avg} remains relatively stable. Fig. 2 summarises what has been described, from a continuous perspective of the fundamental period, by highlighting an increase in bias (i.e. the fitted slope) with the fundamental period of the SDOF systems considering $Sa(T)$, whereas it remained stable with Sa_{avg}, as has also been noted in past literature. This result highlights the need to move away from $Sa(T)$ in the response estimation of these structures and use more robust IMs like Sa_{avg}.

3. Dynamic response quantification

3.1. Methodology

The development of empirical relationships, or demand-intensity models, for a certain typology and the ability to relate the force-deformation capacity (i.e. pushover curve) to its dynamic counterpart, stems from dynamic response characterisation of SDOF oscillators with known pushover backbone parameters [15,55,56]. A similar approach was adopted by Nafeh *et al.* [21] for non-ductile infilled RC frames with infills and considered IDA as the procedure for dynamic capacity quantification using representative SDOF systems. However, considering the shortcomings of IDA briefly noted in Section 2, this study instead employed cloud analysis and Sa_{avg} as the IM.

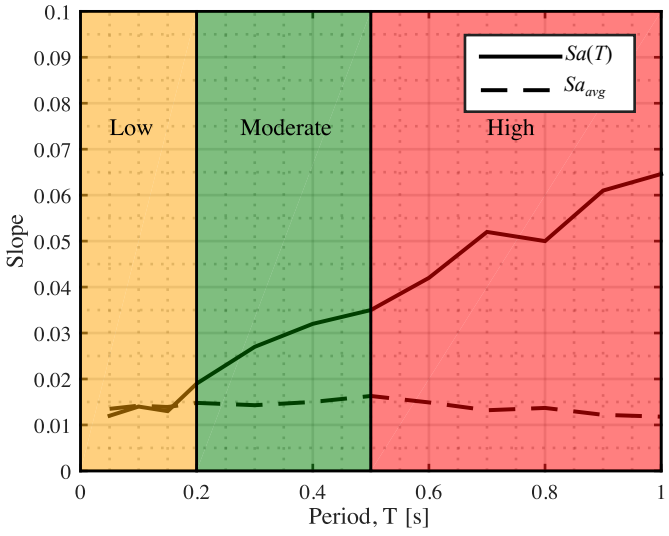

Fig. 2. Depiction of the overall trend of bias (i.e. slope) with the evolution of the fundamental period of the SDOF system for $Sa(T)$ and Sa_{avg}.

To examine these structures, some assumptions about the static pushover's multilinear backbone parameters are needed. Fig. 3 illustrates these, where two considerations are made to account for the failure mode in non-ductile infilled RC frames. In the case of existing RC frames with masonry infills, the infill panels' collapse tends to occur at a very low drift in a single storey meaning that the subsequent response will be more of a soft-storey response in the critical storey, but with significant stiffness remaining at the other non-critical storeys. The use of two pushover curves (Fig. 3) intends to capture these two states of response and increase the robustness of the numerical model through the inclusion of the period-elongation effect when transitioning between stiffnesses and thus realistically mimicking the hysteretic behaviour. This type of approach was also adopted by Dolsek and Fajfar [14,15] for the development of their simplified approach, for example.

The steps followed in the development of demand-intensity models are shown in Fig. 4 and are described as follows:

Step 1: Generate a large set of representative SDOF systems with varying backbone parameters. For this, a representative library of SDOF oscillators generated by Nafeh et al. [21] was used. Then, the static response parameters (i.e. base shear, V_b^* and displacement, Δ^*) for each sampled SDOF system were normalised by the nominal force and displacement values as per Equation (2) and Equation (3) to obtain the static strength ratio, *R*, and ductility demand, μ. It is noted that, compared to similar past studies, the traditionally-employed strength ratio term *R* is replaced by ρ to differentiate between the strength ratio when using $Sa(T_1)$ as the IM from Sa_{avg} being used here. This term ρ is also closely related to the spectral shape parameter *SaRatio* described by Eads et al. [58], for example.

$$R = \frac{V_b^*}{V_{b,y}^*} \tag{2}$$

$$\mu = \frac{\Delta^*}{\Delta_y^*} \tag{3}$$

where V^*_b and $V^*_{b,y}$ are the base shear and yield nominal force of the SDOF system, respectively, and Δ^* and Δ^*_y are the corresponding displacement values, as shown in Fig. 3.

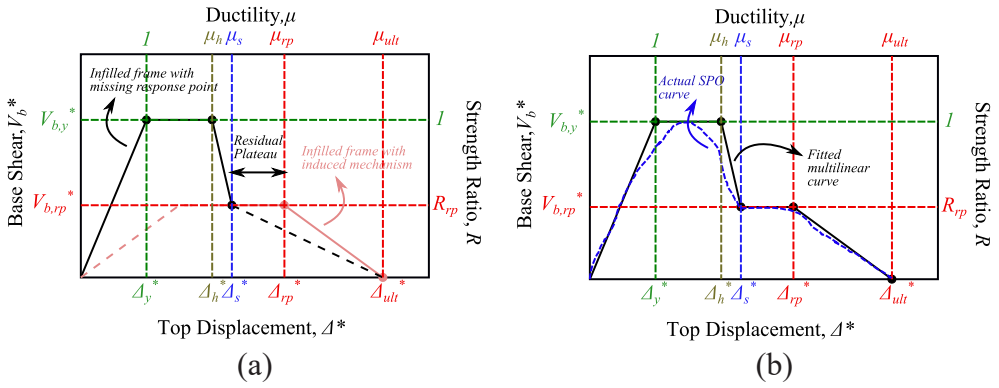

Fig. 3. Multilinear static pushover curve definition of the SDOF systems accounting for the infill contributions to the global system and the formation of the inelastic mechanism for (a) the development of the simplified tool and (b) during the application of the simplified tool.

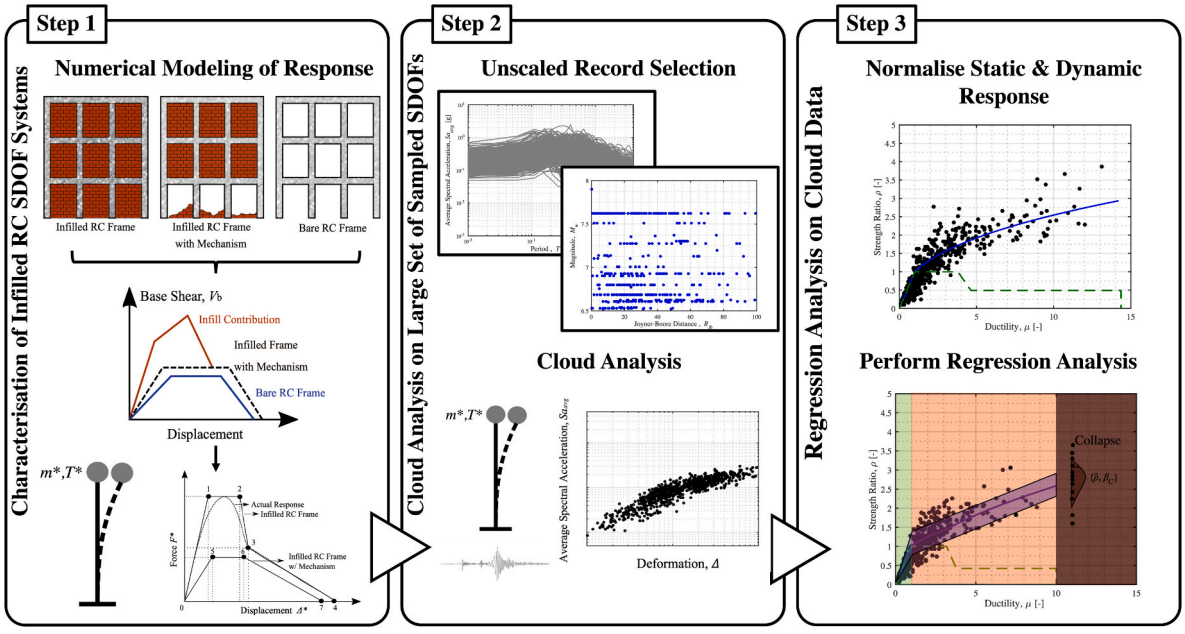

Fig. 4. Workflow followed for the development of the data required for the empirical response quantification.

Step 2: Select a suitable suite of ground motions to develop the demand-intensity models. This was performed in a stratified manner [59] where magnitude-distance bins were defined initially and *n* records were selected. Cloud analysis was performed on each SDOF system to ensure that the EDP-IM response (i.e. demand-intensity model) followed the recommendations of Jalayer et al. [53]. With these cloud analysis results for each SDOF system, the IM described via Sa_{avg} and the structural response in terms of Δ^* was logged in each case.

Step 3: Using the cloud analysis results from Step 2, normalise the deformation and IM levels (i.e. Δ^* and Sa_{avg}) to obtain the dynamic strength ratio, ρ, and ductility, μ. For each record, the Sa_{avg} value corresponding to the SDOF oscillator's period of vibration, T^*, was calculated as:

$$Sa_{avg} = \left(\prod_{i=1}^{N} Sa(c_i T^*) \right)^{1/N} \tag{4}$$

where c_i represent $N = 10$ number coefficients in the range of 0.2 and 3.0, as per Eads et al. [44]'s definition. The ductility was computed as per Equation (3) and the dynamic strength ratio, ρ, was computed using the SDOF's yield spectral acceleration, Sa_y, as follows:

$$\rho = \frac{Sa_{avg}}{Sa_y} = \frac{Sa(T)/SaRatio}{Sa_y} \tag{5}$$

$$Sa_y = \frac{4\pi^2 \Delta_y^*}{T^{*2} g} = \frac{V_{b,y}^*}{m^* g} \tag{6}$$

3.2. Fitting of empirical relationships

Upon the identification of the normalised parameters, a two-step regression analysis was performed similar to other simplified tools, such as SPO2IDA. The first step determines a functional form relating the dynamic strength ratio, ρ, and the ductility demand, μ, resulting in coefficients for each SDOF oscillator. The second step involved the introduction of the period of the SDOF system, T^*, and other relevant strength parameters to relate these properties to the set of coefficients identified in the first step. For each SDOF oscillator, the response was filtered into non-collapsing and collapsing cases and the two-step regression analysis was carried out for both, as discussed below. The numerical collapse was defined as exceeding a lateral displacement in the SDOF systems corresponding to a roof drift of 10% in the MDOF systems. This definition represents a conservative threshold for the

dynamic analysis routine and exceedance of this threshold means the analysis can be confidently considered a collapse case, as discussed in O'Reilly et al. [60].

3.2.1. Non-collapse cases

Following the identification of the normalised demand-intensity model (i.e. ρ - μ_{dyn}) for the non-collapse cases, a bilinear regression was performed. Fig. 5 illustrates an example plotted in logspace in Fig. 5 (a) alongside its backbone characteristics in linear space in Fig. 5(b). The bilinear regressed model identifies the median demand-intensity model of an SDOF oscillator (solid blue line in Fig. 5) and its inherent dispersion or uncertainty (blue shading in Fig. 5) associated with record-to-record variability. It is worth mentioning that while a linear fit represents a rather convenient simplification of the statistical regression model chosen herein, the use of the single linear fit may not be appropriate over the entire range of structural response. In fact, as per O'Reilly and Monteiro [61], a bilinear demand-intensity model is more suitable for structural systems like infilled RC frames where the response is dictated by the sudden rupture and collapse of the infills at some storeys. The change in response was identified due to the formation of the inelastic mechanism and is observed here in Fig. 5, where two response branches were identified: elastic and inelastic mechanisms. A bilinear regression was performed first for a purely elastic system until the yield point, which corresponds to the local collapse of infills at one or more levels, and the inelastic mechanism ensued. The point at which the structural response transitions into a bilinear response was assumed as the yield nominal base shear, $V^*_{b,y}$, corresponding to an $R = 1$, following Fig. 3.

With the data in Fig. 5, a two-step regression was carried out to relate the parameters of the fitted demand-intensity model to the pushover response parameters and modal properties. First, a functional form relating the median dynamic strength ratio, $\widehat{\rho}_{NC}$, and the ductility, μ, was identified for the non-collapse cases. The bilinear demand-intensity model adopted is a combination of two linear models in the logspace, described by:

$$\mu \leq 1,\ \widehat{\rho}_{NC} = \exp(a_1 \ln(\mu) + b_1),\ a_1 = 1;\ b_1 = b_2 \tag{7a}$$

$$\mu > 1,\ \widehat{\rho}_{NC} = \exp(a_2 ln(\mu) + b_2) \tag{7b}$$

The branch corresponding to the post-elastic response ($\mu > 1$) of the system was fitted first and the slope and intercept, a_2 and b_2, corresponding to the linear fit in logspace were identified. Subsequently, the regression model corresponding to the elastic response ($\mu \leq 1$) was characterised following the identification of the post-elastic parameters to ensure a smooth transition between both branches of response. Next, the second step of the regression analysis was carried out, where the parametric relationship between the dynamic and strength properties of the equivalent SDOF system and the coefficients a_1, a_2 and b_1, b_2 was defined. As highlighted earlier in Section 3.2, the second step of the regression and the consequent relationships derived in Equations (8)–(11) aim at characterising a unique response corresponding to buildings with dissimilar response parameters. Moreover, the introduced parameters and their complex relationships were the results of observation in trends where the error and dispersion are minimised. Regarding the elastic branch of the response, the values of a_1 and b_1 were 1 and 0, respectively, simply representing an elastic system until the inelastic mechanism develops. In other words, the strength ratio is equal to ductility for $\mu \leq 1$. Following this, Equation (8) and Equation (9) describe the relationships for the coefficients a_2 and b_2 representing the second branch of the bilinear response.

$$a_2 = 0.704 \left(\frac{T^*}{V^*_{b,y} \Big/ W^*} \right)^{0.1595} - 0.239 \tag{8}$$

$$b_2 = 1.813 \left(\frac{V^*_{b,rp}}{W^*} (\mu_{rp} - \mu_S) \right)^{0.0473} - 1.98 \tag{9}$$

$V^*_{b,y} \Big/ W^*$ is the nominal base shear coefficient (i.e. yielding and subsequent inelastic mechanism); $V^*_{b,rp} \Big/ W^*$ is the coefficient corresponding to the residual strength capacity of the SDOF system and its total seismic weight, W^*. The ductilities, μ_{rp} and μ_S are shown in Fig. 3 and represent the softening and end of residual plateau points of the normalised static pushover curve, respectively. The coefficients were derived as a function of the independent variables showing the highest correlation for salient response branches, such as the period, T^*, the base shear coefficient, V^*/W^*, and the ductility demand corresponding to the residual plateau, μ_{rp}. The relationship between the coefficients and the SDOF properties are illustrated in Fig. 6. The use of normalised values is beneficial in avoiding overfitting in the predictive functional form, ensuring the representativeness of the fitted coefficients, and without any information leakage in the predictive model.

The goodness-of-fit parameters, such as the sum of the squares due to error (SSE), R-square (R^2) and root mean square error (RMSE) are reported in Table 1. These parameters infer, respectively, the total deviation of the response values from the regressed fit to the actual data, the correlation between the predicted response values and the actual data, and the estimate of the standard deviation of the random component in the data. The notion of standard deviation in the context of the

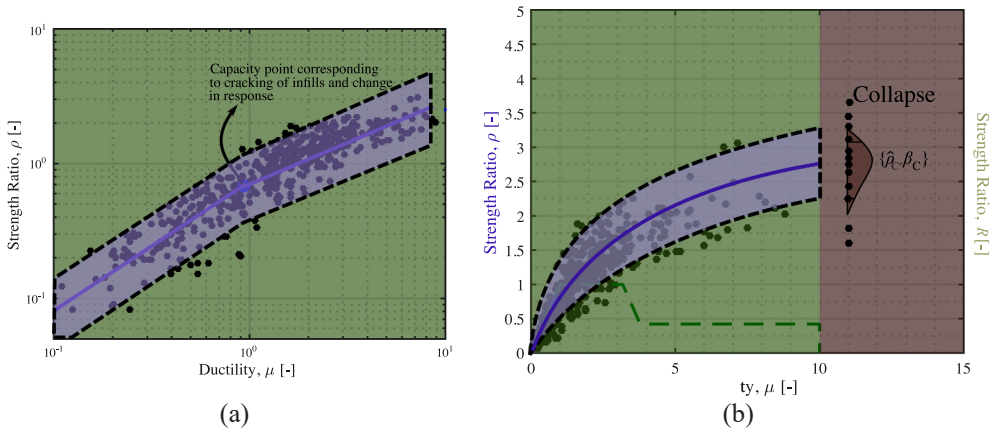

Fig. 5. Example of response branch fitting methodology where (a) the bilinear fit in log-space of elastic and inelastic mechanism response (b) the corresponding dynamic capacity curve in linear space. (Note: black scatter points are cloud analysis runs; solid blue lines are the regressed bilinear fits; green dashed line is the normalised static response curve; and the blue shaded region is the corresponding dispersion ($\pm\beta_{NC}$) of the data).

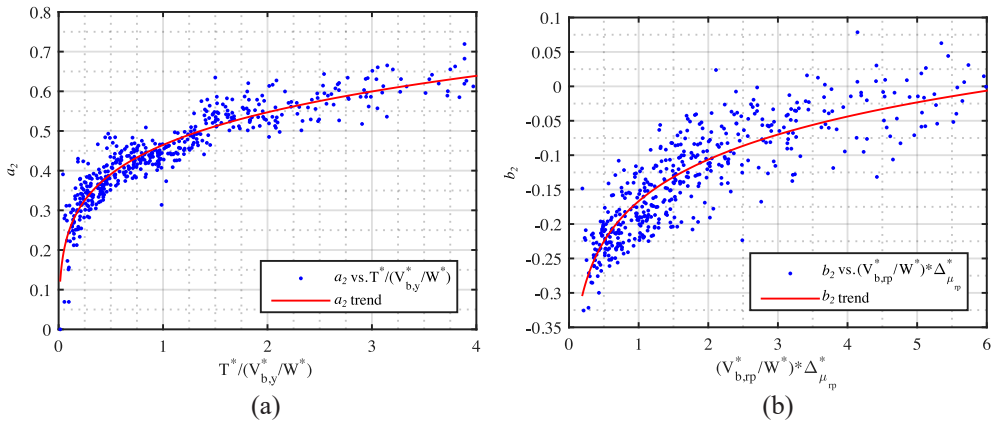

Fig. 6. Predictive trends for the coefficients a_2 and b_2.

Table 1
Goodness-of-fit results for coefficients a_2 and b_2.

Coefficient	Goodness-of-Fit Metric		
	SSE	R^2	RMSE
a_2	0.8187	0.8819	0.04026
b_2	0.8801	0.7873	0.04175

goodness-of-fit metrics corresponds to the uncertainty in the regressed functional form associated with the coefficients a_2 and b_2. It can be seen from these parameters that the adopted model represents the coefficients well.

The dispersion in ρ_{NC} for the non-collapsing cases, denoted β_{NC}, refers to the standard deviation of the cloud data from the regressed demand-capacity model and thus explains the difference in predicted and observed values. It considers the record-to-record variability in the cloud analyses only and was denoted via the shaded blue regions in Fig. 5. Fig. 7 illustrates the range of observed dispersion values following the fitting of the demand-intensity model. A fixed value of $\beta_{NC} = 0.27$ was assigned as it was the most frequently observed value for all cases, with no distinct trend with structural strength or ductility parameters observed when investigated.

3.2.2. Collapse cases

Using the same data described in Section 3.2.1, the collapsing cases were identified and were used for fitting here, as illustrated in Fig. 5(b). Since the ductility demand is no longer of direct interest, but rather the binary case of collapse or non-collapse, a single-value of the median strength ratio corresponding to collapse, $\widehat{\rho}_C$, and the associated dispersion, β_C, were subsequently identified for each SDOF system. Following the identification of $\widehat{\rho}_C$ for each SDOF oscillator, the correlation with the strength and ductility parameters was investigated. To this end, a linear expression was obtained as a function of the parameters illustrated in Fig. 3, and is described as follows:

$$\widehat{\rho}_C = -1.62\,c + 3.32 \tag{10}$$

$$c = \left(1 - \left(\frac{V^*_{b,rp}}{V^*_{b,y}}\right)\frac{(\mu_{rp} - \mu_S)}{\mu_{ult}}\right) \tag{11}$$

The parameters found to be most influential in describing the collapse capacity of the system include the drop in lateral capacity (i.e. the ratio of residual to yield strength), the ductility of the residual strength plateau and the ultimate ductility, μ_{ult}. The ratio of the strengths was deemed an adequate parameter for the collapse capacity as it reflects the residual load-bearing capacity of a structural system. The ductility demand is an essential indicator of the inelastic deformation sustained by the structural system before collapse. Fig. 8 illustrates this further where the trend between $\widehat{\rho}_C$ and the coefficient c is shown. The goodness-of-fit metrics for this model are reported in Table 2 and reflect

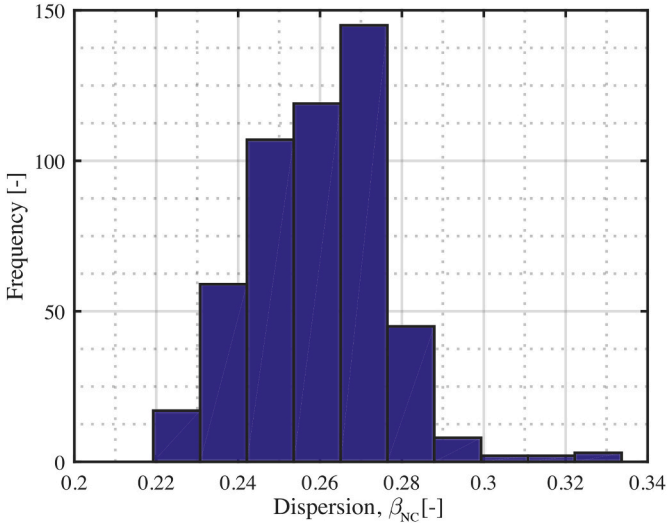

Fig. 7. Distribution of the observed dispersion values (β_{NC})

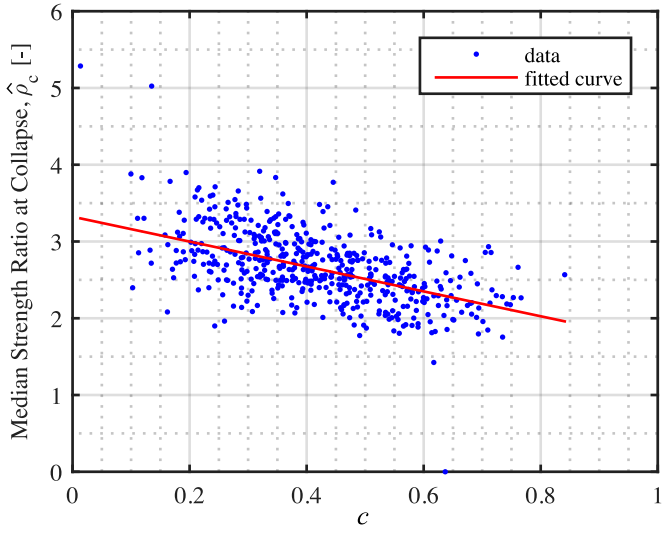

Fig. 8. Linear regression of the median dynamic strength ratio at collapse and the dimensionless coefficient.c

Table 2
Goodness-of-fit results for coefficient, *c*.

Goodness-of-Fit Metric		
SSE	R^2	RMSE
1.55	0.9865	0.05546

a relatively good fit, where the error is minimised and the predictive capacity of the statistical model is high.

The collapse dispersion associated with record-to-record variability, β_C, was subsequently identified. Fig. 9 illustrates the calculated values of β_C versus the median strength ratio observed at collapse, where no discernible trend is evident, nor was any trend for other parameters. Consequently, β_C was fixed as the median of the observed dispersions for each SDOF at collapse as $\beta_C = 0.375$.

3.3. Validation

Following the description of the fitted models, this section presents a brief validation of the demand-intensity parameters with an independent set of 50 equivalent SDOF systems and ground motion records. Cloud analysis was performed and the median intensities corresponding to a performance limit of 1.0% top drift and collapse are plotted in Fig. 10 with the associated dispersions. They are compared with the predicted median intensities and dispersions from Sections 3.2.1 and 3.2.2. Fig. 10 illustrates a very good agreement, both in terms of the medians and the dispersions. This shows the capability of the tool in predicting the performance from the onset of inelastic deformation up until global collapse of these structural systems, which will be further demonstrated on sets of case-study archetype buildings in Section 5.

3.4. Application

With these empirical models fitted in Section 3.2 and validated in Section 3.3 to quantify the collapse and non-collapse performance of non-ductile infilled RC frames, this section briefly describes their implementation in a practical setting. Before the application of the proposed tool, non-linear static and eigenvalue analyses are needed. Then, the global capacity parameters corresponding to the thresholds of the response branches (e.g., elastic-hardening-softening-residual plateau-ultimate deformation) are identified. As such, a multi-linearisation of the SPO curve (i.e., base shear vs roof displacement) corresponding to the MDOF system is performed. The global capacity parameters (i.e., response branch thresholds or performance points) necessary for the application of the simplified tool are highlighted in Fig. 11. Subsequently, the MDOF system is then transformed via Γ to an equivalent SDOF system with an equivalent backbone definition. The backbone corresponding to the SDOF system (i.e. base shear vs top displacement) is then normalised (i.e. R vs μ) to the nominal yield force of the SDOF system and corresponding top displacement at yield. The proposed simplified tool then computes the necessary coefficients needed for the regression and calculates consequently the normalised dynamic capacity curves (i.e. ρ vs μ).

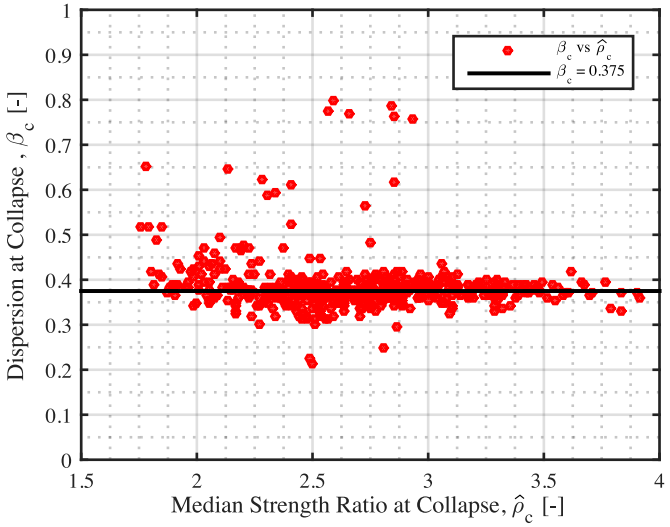

Fig. 9. Observed values of dispersion for the collapse cases.

For the case of non-collapse, a limit state (LS) associated with a value of roof displacement, Δ, or a ductility demand, μ, in the system is first defined. Following the normalisations illustrated in Fig. 3, the normalised ductility demand is established for this LS. Having conducted a static pushover analysis on the structure, the other parameters shown in Fig. 3 are also quantified. Using the model described in Section 3.2.1, the median strength ratio required to exceed this limit state LS is computed via Equation (7a) as $\hat{\rho}_{NC}$ with an associated dispersion of $\beta_{NC} = 0.27$. To convert this median strength ratio to a median ground motion intensity in terms of Sa_{avg}, denoted $\hat{\eta}_{NC}$, this is computed as per Equation (12):

$$\hat{\eta}_{NC} = \hat{\rho}_{NC} Sa_y \Gamma \tag{12}$$

where Sa_y is defined as per Equation (6) and Γ is the transformation factor to revert the equivalent SDOF oscillator to the corresponding MDOF system. The use of the first-mode of vibration, whose modal masses is typically 85–90% of the total, neglects the impact of higher modes. Other uncertainties and sources of error may include: the assumption of a constant modal shape corresponding to the first (elastic) mode of vibration; the selected regression model and the associated fitting errors; other analysis-based uncertainties due to the variability in backbone parameters due to building-to-building variability or the uncertainty due to the record-to-record variability. None of these are deemed significant but are accepted as part of the simplifying process to make such advanced calculations accessible to practitioners. Thus, it is computed via the fundamental modal properties obtained through eigenvalue analysis of the structural model using Equation (13).

$$\Gamma = \frac{\sum_i m_i \varphi_i}{\sum_i m_i \varphi_i^2} \tag{13}$$

where m_i and φ_i represent the mass and normalised first mode shape at a given floor *i*. With the median intensity and dispersion known (i.e. $\hat{\eta}_{NC}$ and β_{NC}), the probability of exceeding this limit state LS for a given value of IM = Sa_{avg} assuming no collapse, $P(LS|NC, IM = Sa_{avg})$, can be computed by assuming a lognormal distribution [30] with Equation (14).

$$P(LS|NC, IM = Sa_{avg}) = \Phi\left(\frac{\ln(\text{Sa}_{\text{avg}}/\hat{\eta}_{NC})}{\beta_{NC}}\right) \tag{14}$$

where Φ represents the standardised Gaussian cumulative distribution function.

For the case of collapse, the same general approach is followed using the model fitted in Section 3.2.2. The median strength ratio required to cause collapse, $\hat{\rho}_C$, is computed via Equation (10) using the same normalised parameters computed from pushover analysis shown in Fig. 3. To convert this median collapse strength ratio to a median ground motion intensity in terms of Sa_{avg}, denoted $\hat{\eta}_C$, Equation (15) is used:

$$\hat{\eta}_C = \hat{\rho}_C Sa_y \Gamma \tag{15}$$

where Sa_y and Γ are the same as before. As per Section 3.2.2, the associated dispersion at collapse is set as $\beta_C = 0.375$ and with both the median and dispersion known (i.e. $\hat{\eta}_C$ and β_C), the probability of collapse for a given value of IM = Sa_{avg}, $P(C|IM = Sa_{avg})$, can be computed by assuming a lognormal distribution with Equation (16).

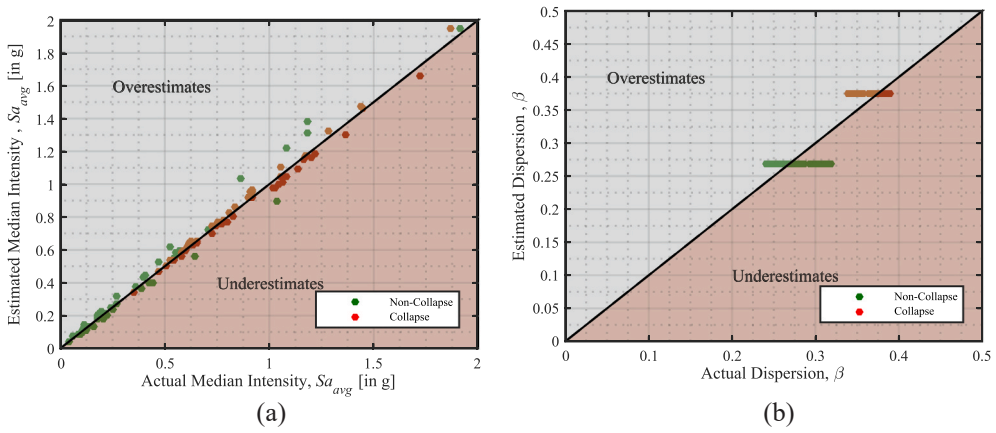

Fig. 10. Comparison of the estimated (using proposed simplified approach) vs actual (using cloud analysis) median intensities corresponding to the non-collapsing performance limit of 1.0% top drift and collapse given in terms of Sa_{avg} and their respective dispersions.

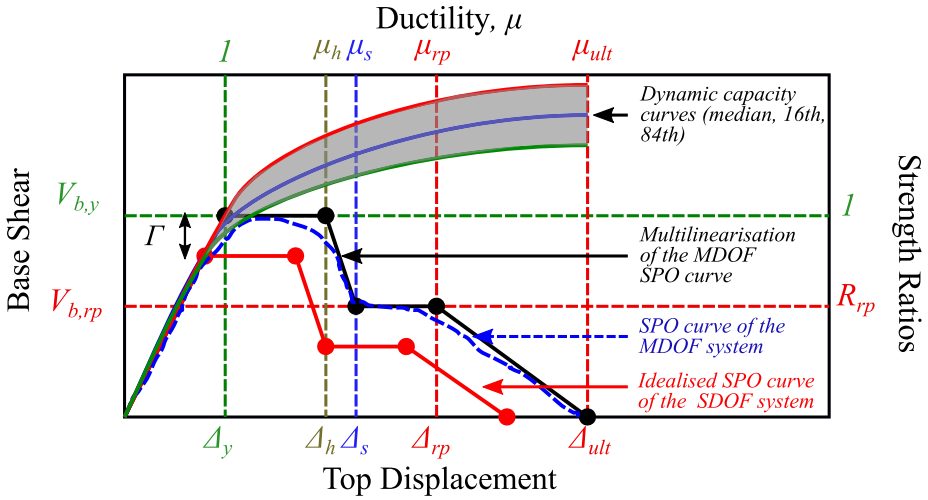

Fig. 11. Application of the proposed simplified tool for the dynamic capacity quantification of the MDOF system.

$$P\left(C\middle|IM = Sa_{avg}\right) = \Phi\left(\frac{\ln\left(\mathrm{Sa_{avg}}/\widehat{\eta}_C\right)}{\beta_C}\right) \tag{16}$$

Knowing the probability of collapse and a given LS exceedance for IM = Sa_{avg}, a more accurate and unbiased estimate of the seismic performance of non-ductile infilled RC frame buildings can be quantified. It is noted that this is done with relative ease following the above approach and can be integrated within a PBEE setting to assess and classify such building typologies. This proposed tool is available at the following GitHub repository: https://github.com/gerardjoreilly/Infilled-RC-Building-Response-Estimation [62].

4. Case study validation

For the validation of the approach developed for non-ductile RC frame structures with masonry infills and proposed in Section 3, four case study buildings pertaining to a database of building models (presented in Appendix A) were analysed. The comparison was performed in terms of the fragility functions developed, which were computed from an extensive dynamic analysis of the numerical models using hazard-consistent ground motions and using the simplified pushover-based approach described in Section 3.4. To this end, two locations in Italy were selected: Napoli, and L'Aquila representing sites of medium and high seismicity, respectively. Buildings 2-D-GLD and 2-D-SDD were located in Napoli, whereas 4-F-GLD and 4-F-SSD were located in L'Aquila. The aim of selecting two different locations was to compare the response estimation of the proposed tool across differing seismicity levels. The case study set of results presented here comprises two building plan layouts (Fig. 12) considering the construction periods identified in Section 4.1, whose design details are summarised in Table 3.

The static response of the case study buildings was computed via a pushover analysis in both principal directions, whose results are reported in Fig. 13 and Fig. 14. These plots were normalised in terms of the strength ratio, ρ, and ductility, μ, described in Section 3.1. The results indicate the evolution in the design norms, with an increase in the strength ratio, ρ, and subsequently the ductility, μ, being observed due to the increase in structural sections and increased reinforcement ratios. For dynamic analyses, a hazard analysis was conducted using the OpenQuake engine [63] considering Sa_{avg} as the IM and the site characteristics presented in Mori et al. [64]. Hazard-consistent ground motion records were selected from the NGA-W2 database using the conditional spectrum approach [49] for Sa_{avg}. and the geometric mean of the two components was considered for the selection. Scale factors for the selected records were limited to 3.5 to mitigate any issues of bias, as previously discussed in Section 2. MSA were conducted for six intensity measure levels to characterise the structural response from initial damage of the masonry infill panels right up to global structural collapse.

For the simplified approach proposed here, the principal direction of the building that exhibited the lowest ductility was used to characterise

Fig. 12. Plan layouts of the case study buildings.

Table 3
Structural properties of the case study buildings.

Case Study Building ID	Number of Frames			Column Sections (cm)	Beam Sections (cm)	Longitudinal Reinforcement Ratios (%)	Transverse Reinforcement (diameter/spacing)	Material Characteristics
2-D-GLD	X	Exterior	2	25 × 25	50 × 30	C: 0.75%–0.98% (φ16)	C: φ6 @150 mm	Smooth Rebars (Aq42, σ = 140 MPa);
		Interior	1	30 × 30		B: 0.21%–0.41% (φ14)	B: φ6 @200 mm	Concrete (σ = 5 MPa);
	Y	Exterior	2					
		Interior	0					
2-D-SSD	X	Exterior	2	30 × 30	50 × 30 (DB)	C: 0.75%–0.98% (φ16)	C: φ8 @150 mm	Deformed Rebars (FeB44k, σ = 260
		Interior	1	35 × 35	30 × 70 (CB)	DB: 0.23%–0.46% (φ14)	B: φ8 @100 mm	MPa); Concrete (σ = 7.5 MPa);
	Y	Exterior	2			CB: 0.82%–0.95% (φ14)		
		Interior	6					
4-F-GLD	X	Exterior	2	20 × 20	55 × 30	C: 0.75%–0.98% (φ16)	C: φ6 @150 mm	Smooth Rebars (Aq42, σ = 140 MPa);
		Interior	1	25 × 25		B: 0.28%–0.46% (φ14)	B: φ6 @200 mm	Concrete (σ = 5 MPa);
	Y	Exterior	2					
		Interior	0					
4-F-SSD	X	Exterior	2	25 × 25	55 × 30 (DB)	C: 0.75%–0.98% (φ16)	C: φ8 @150 mm	Deformed Rebars (FeB44k, σ = 260
		Interior	1	30 × 30	35 × 75 (CB)	DB: 0.32%–0.51% (φ14)	B: φ8 @100 mm	MPa); Concrete (σ = 7.5 MPa);
	Y	Exterior	2			CB: 0.59%–0.71% (φ14)		
		Interior	0					

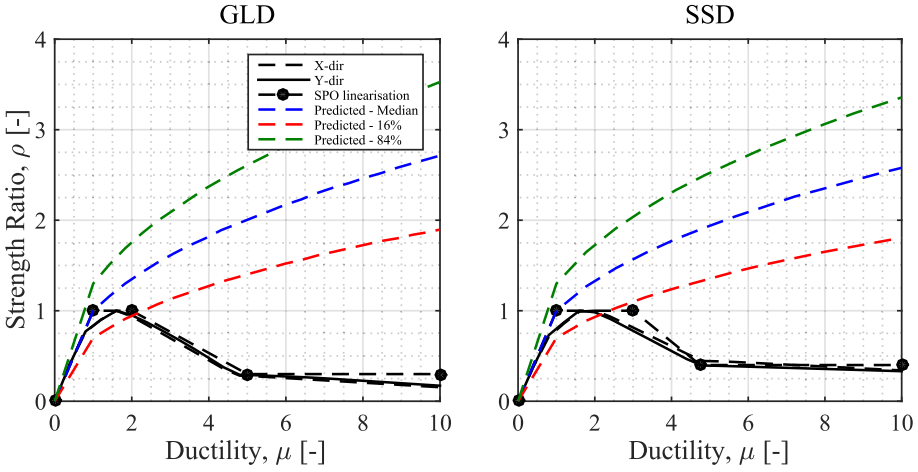

Fig. 13. Normalised static pushover analysis curves for the 2-D-GLD and 2-D-SSD case study buildings shown together with dynamic capacity estimation.

the dynamic response of the building. Moreover, the base shear and roof displacement values were used as input along with the first-mode shape extracted from an eigenvalue analysis and the corresponding storey masses to a spreadsheet-based tool implementing the approach presented in Section 3 and available online [62].

To evaluate the fragility functions predicted by the proposed simplified approach compared to those derived from extensive analyses with ground motion records, two limit states were considered. These corresponded to a peak storey drift of 1% along the height of the structure and the collapse of the building. The median intensities in terms of Sa_{avg} and the associated dispersions were identified and are listed in Table 4 along with the error with respect to the MSA values. The corresponding fragility functions are plotted in Fig. 15 and Fig. 16 and illustrate an excellent matching between MSA and the proposed simplified approach presented in Section 3.4 this study. This can be observed in the matching between the median intensities computed for

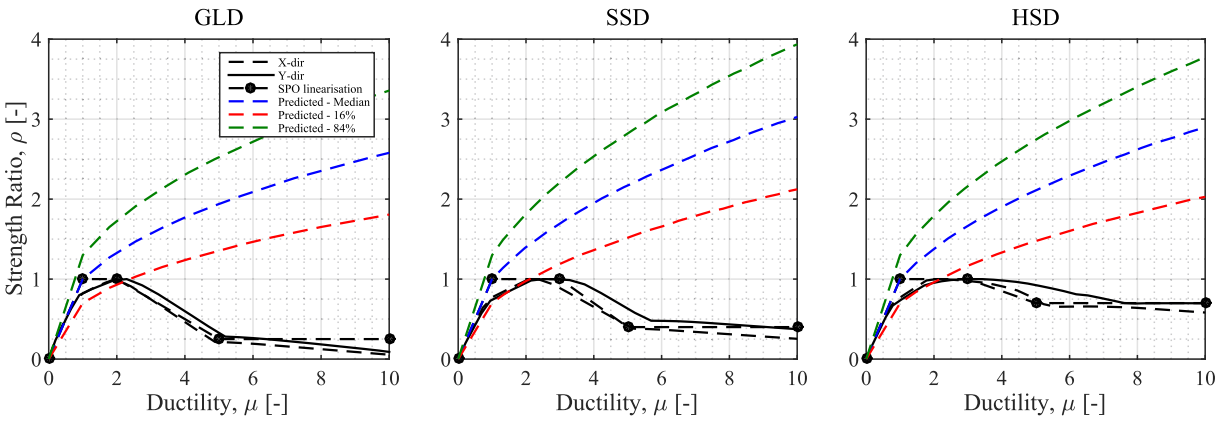

Fig. 14. Normalised static pushover analysis curves for the 4-F-GLD and 4-F-SSD case study buildings shown together with dynamic capacity estimation.

Table 4
Comparison of the median intensity and dispersion values for non-collapse and collapse.

Non-Collapse					
Case Study ID	Multiple Stripe Analysis		Simplified Approach		Error in $\widehat{Sa_{avg}}$
	$\widehat{Sa_{avg}}$ [g]	β_{NC}	$\widehat{Sa_{avg}}$ [g]	β_{NC}	
2-D-GLD	0.51	0.33	0.58	0.27	13.72% (+)
2-D-SSD	0.57	0.31	0.62		8.77% (+)
4-F-GLD	0.43	0.34	0.38		11.63% (-)
4-F-SSD	0.52	0.30	0.47		9.61% (-)
Collapse					
Case Study ID	Multiple Stripe Analysis		Simplified Approach		Error in $\widehat{Sa_{avg}}$
	$\widehat{Sa_{avg}}$ [g]	β_C	$\widehat{Sa_{avg}}$ [g]	β_C	
2-D-GLD	0.90	0.24	0.95	0.375	5.55% (+)
2-D-SSD	1.00	0.25	1.05		5.00% (+)
4-F-GLD	0.73	0.25	0.75		2.74% (+)
4-F-SSD	0.88	0.18	0.95		7.95% (+)

each limit state of the buildings, with an error generally less than 10% (Table 4). Similarly in terms of the dispersion values, where the proposed values match the computed values quite well. The proposed approach showed only slightly conservative estimates in terms of collapse fragility regarding the GLD and SSD designed buildings. Considering the exceedance of 1% peak storey drift, the proposed approach reported only slight errors for the GLD and SSD cases. The comparison presented herein illustrates the accuracy of the proposed approach to be generally employed for such typologies of different building height and across different seismicity types

Subsequently, the fragility function parameters corresponding to the median collapse intensities and associated dispersions for the remaining GLD and SSD archetype buildings of the database presented are in Figure 20 and 21, respectively. These parameters correspond to the results of the multiple stripe analysis conducted on two different sites (i.e., Napoli and L'Aquila) corresponding to two levels of seismicity. The median collapse intensities and the associated dispersion are then compared with respect to the intensities obtained from the simplified tool. The tool's robustness in estimating the median intensities corresponding to collapse is evident considering all the case study building models presented. Furthermore, the tool slightly overestimates the values of the associated uncertainty (Fig. 18) highlighting a conservative aspect to the response estimation, which could be further explored in future research.

Following the good matching of results highlighted in Fig. 17, it is evident that any errors associated with the simplifying assumptions (e.g., use of the transformation factor, Γ, or the Sa_y-constrained normalisation for the dynamic strength ratio) did not appear to have any significant impact on the accuracy of the tool when applied to numerous representative structural models.

5. Summary and conclusions

The accurate assessment and evaluation of reinforced concrete (RC) structures with masonry infills due to seismic action remains an open challenge in modern earthquake engineering. The performance quantification of this typology is of importance to practitioners and decision-makers considering the prevalence of such typology in the southern European building stock and their complex behaviour. In risk-based analyses, the proper characterisation of infilled RC buildings through proper numerical modelling of the response up to dynamic instability (i.

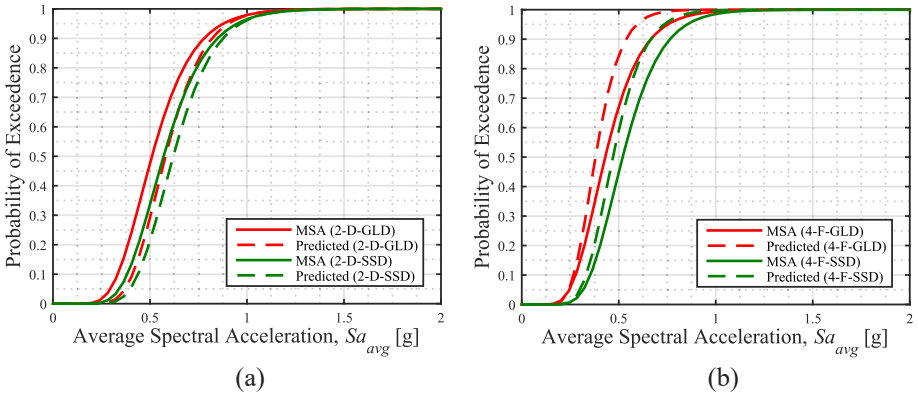

Fig. 15. Fragility curves for to exceedance 1% storey drift along the building height derived from MSA and the proposed simplified approach for each building (a: 2-D-GLD and 2-D-SSD; b: 4-F-GLD and 4-F-SSD).

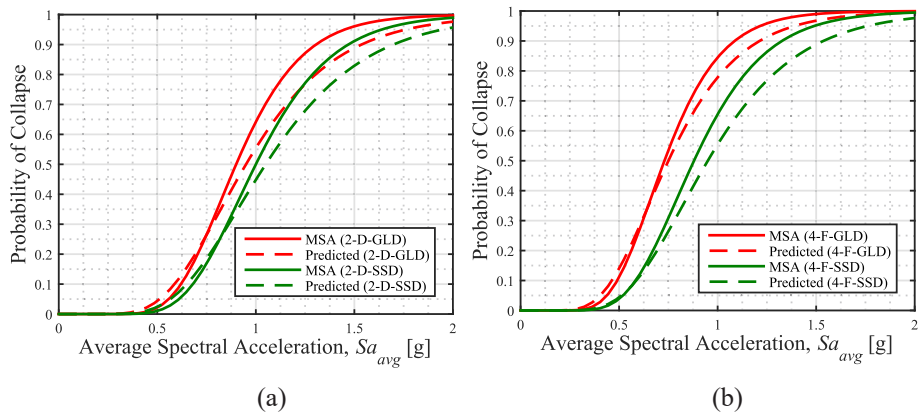

Fig. 16. Collapse fragility curves corresponding to MSA and the proposed simplified methodology for each building.

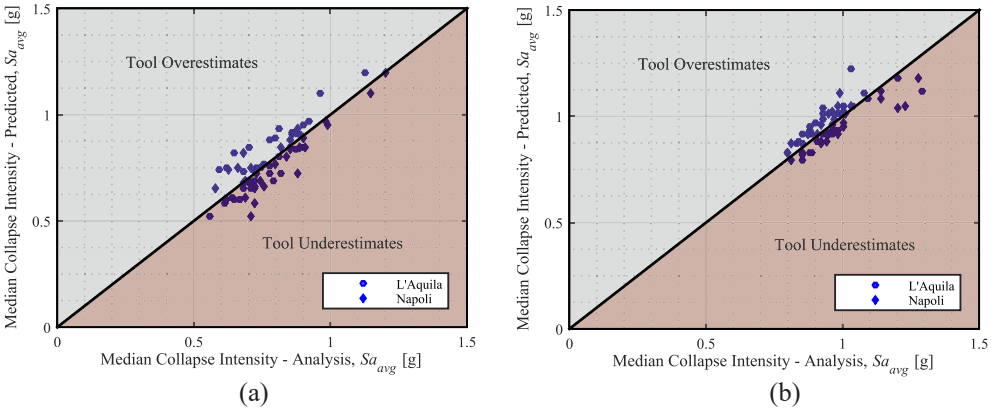

Fig. 17. Comparison of the median collapse intensity obtained from traditional analysis (MSA) considering the case study sites and the estimated intensities from the response evaluation tool (a: GLD, b: SSD).

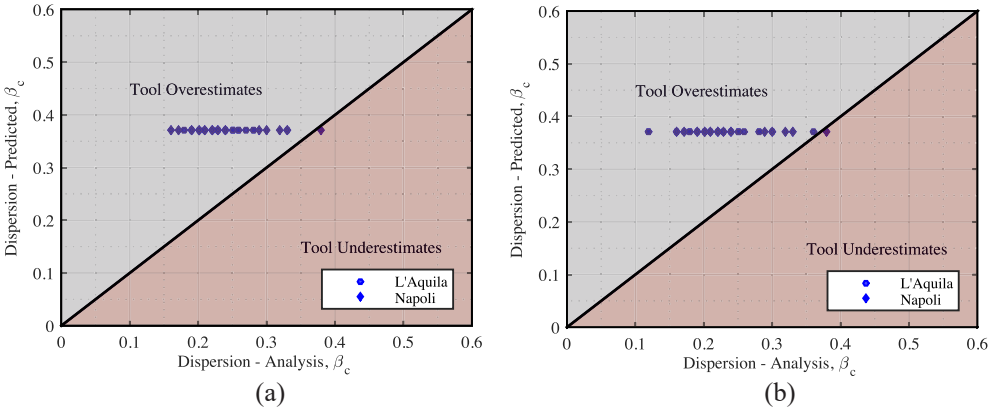

Fig. 18. Comparison of the dispersions associated to the median collapse intensity obtained from traditional analysis (MSA) considering the case study sites and the estimated intensities from the response evaluation tool (a: GLD, b: SSD).

e. collapse) is essential. Furthermore, non-linear dynamic analyses such as incremental dynamic, multiple stripe and cloud analysis are computationally expensive in terms of time and effort. Moreover, these dynamic analyses can potentially introduce bias in the results obtained due to high scaling factors and the choice of suitable intensity measures. To this end, this paper introduced several items in an attempt to facilitate the needs of risk modellers, and to ease the burden of computationally expensive procedures and address their limitations. Some of the main outcomes of this study are:

- A simplified seismic assessment approach based on non-linear static analysis (i.e. pushover) to estimate the capacity of non-ductile infilled RC frame buildings has been presented and built into a simplified tool, providing ease of applicability for future users;
- The cloud analysis performed in the development phase of the proposed approach addresses the issue of potentially biased response predictions introduced through high ground motion scaling factors and poor choice of intensity measure encountered when following existing methods;

- Verification of the proposed methodology to derive the empirical fits was first conducted on a randomly sampled set of representative single degree of freedom oscillators;
- A database of three-dimensional infilled RC archetypes representative of notable phases of existing Italian construction was developed and numerically modelled in OpenSees;
- Further validation was performed on case-study buildings located on two different sites in Italy for limit states representing moderate inelastic response and full collapse of the buildings, with the proposed approach exhibiting high accuracy in all cases;
- Lastly, the capability of the tool in accurately quantifying the collapse capacity renders it a potential improvement to be implemented in risk classification guidelines such as Sismabonus in Italy, specifically for the infilled RC typology.

Declaration of competing interest

The authors declare that they have no known competing financial interests or personal relationships that could have appeared to influence the work reported in this paper.

Acknowledgments

The work presented in this paper has been developed within the framework of the project "Dipartimenti di Eccellenza", funded by the Italian Ministry of Education, University and Research at IUSS Pavia. The authors would like to acknowledge the contribution of Arch. Ing. Tereza Nádeníková and Arch. Ing. Barbara Ferma during the conception of the case study buildings presented in this study.

Appendix A. Development of archetype database for non-ductile infilled RC buildings

RC structures with masonry infills are one of the most prevalent typologies of the southern European region. In Italy, the population and housing statistics from ISTAT (Istituto Nazionale di Statistica) [65] provide important information on the prevalence of a structural typology as part of the regional building stock (Figure 19). The distribution of buildings was also found to be consistent with the findings of Crowley et al. [66]. This typology was widely employed given its low construction cost, reliability with fire and moisture along with their beneficial thermal and acoustic insulation properties. Masonry infills were considered as non-structural elements and their interaction with the surrounding structural elements was neglected during the design process. However, the occurrence of earthquake events over the last century has highlighted the detrimental effects of not considering the infill partitions as part of the structural design. Experimental and analytical studies [67–72] have outlined the effects of masonry infills on the global lateral response of the structural system. These effects are characterised by a significant addition in lateral stiffness and a sudden drop in lateral strength with the rupture of infills at one or several storeys. Considering the prevalence of this typology in Europe and Italy, this work aims to develop a database of archetypical buildings that may be considered representative of this existing stock found throughout Italy and Southern Europe.

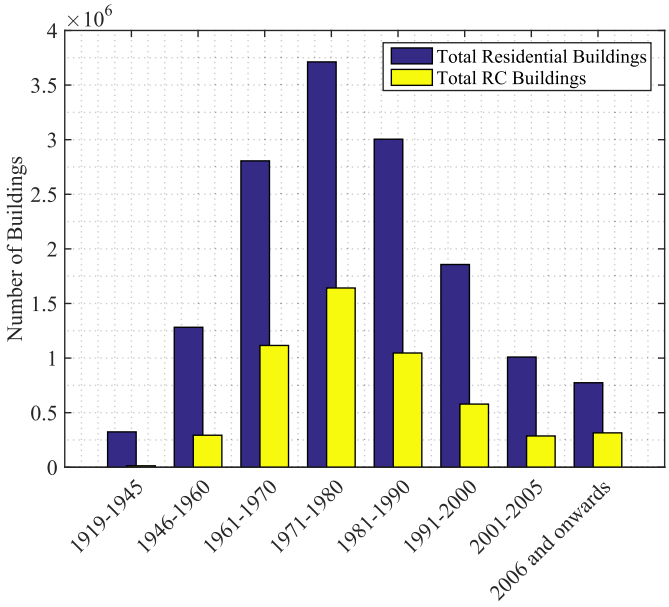

Fig. 19. Evolution of the Italian built environment with emphasis on the percentage of RC buildings with respect to the total residential building stock [65].

A1. Building characteristics

Assessing the seismic performance generally requires analyses performed on building models widely considered representative of the building class under scrutiny, generally referred to as archetypes. Archetype building models are implemented within a PBEE framework [73] to provide further contribution and validation to existing fragility and vulnerability components and consequently a comprehensive loss assessment. Guidelines such as FEMA P695 and ATC63 [74] outline the requirements to be considered when characterising archetype building models, which are briefly reported here. Archetype configurations should be conceived and modelled based on key design features; these design variables must be sufficiently broad to satisfy the feasible range of design requirements. Said variables include features such as period of construction, corresponding design practice, gravity and lateral load-bearing structural system and variability in material properties, type of occupancy and designated use, building height, elevation and plan configuration.

In addition to the identification of the design space features, the characterisation of a building class depends on the definition of key architectural features such as span distributions, compartmentalization of the living space, type of occupancy and designation of storey heights must be accounted

for. To this end, this information is incorporated here and further information can be extracted from the ISTAT housing database. Characteristics such as storey height and floor space area per dwelling are reported in Figure 20. These values are combined with the findings of Perrone et al. [75] regarding the expected lengths and number of bays to demonstrate values for geometrical characteristics representative of typical Italian construction.

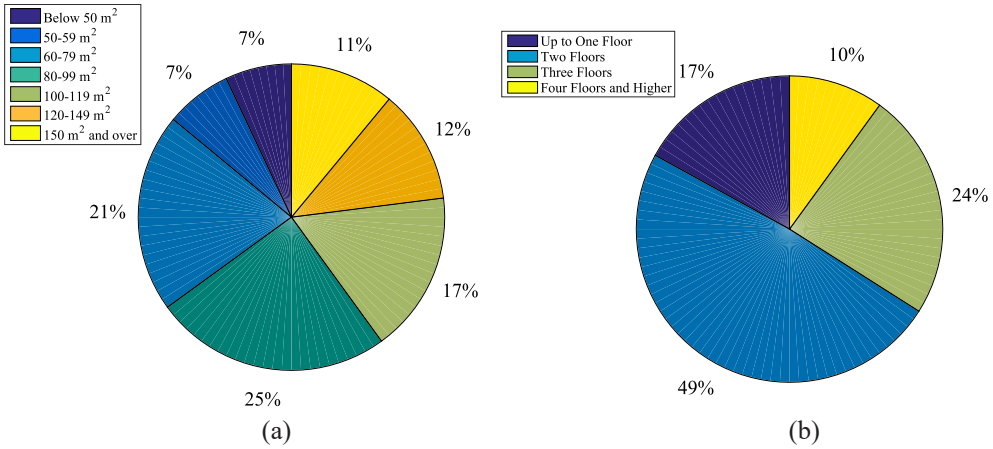

Fig. 20. Percentage of dwellings disaggregated per surface area and per total number of floors.

To fully identify the most prominent features of a regional design space, a further inspection of the regional design or construction practice was necessary. The temporal evolution of the design and building properties is an important aspect in properly characterising the behaviour of a structural typology of interest. Geographical specifications and conditions (i.e. building material, design methodology specific for a region, etc.) in which the buildings were conceived should be accounted for. Nowadays, the Italian design code [2] has been significantly improved with the use of limit states, ductility classes and importance classes of the structure itself, among other facets. Before the introduction of modern seismic provisions around the 1970s in Italy, buildings were mainly designed to resist gravity loads only with no consideration of ductile detailing or capacity design principles. These buildings were mainly designed using the Royal Decree 2229/39 [76] with complementary references [77,78], utilising the allowable stress method in design. Design features of these gravity load designed (GLD) buildings include frames spanning in one direction only, the use of smooth rebars and concrete with relatively low yield and compressive strengths, poor transverse detailing and shear reinforcement, inadequate detailing of the beam-column joints.

The period between the mid-1970s and 1980s witnessed the implementation of the equivalent lateral force (ELF) method. The ELF method requires a seismic coefficient, defined as around 7%–10% by Crowley et al. [79] and other studies [80–82]. This design approach was coupled with the allowable stress method for the dimensioning and detailing of structural members. The main guidelines were L. 1086/71 [83], D.M. 40/1975 [84] and D.M. 108/1986 [85]. Features of this sub-standard design (SSD) practice at the time include frames spanning in one (or both) directions, the use of deformed rebars and concrete with moderate yield and compressive strengths respectively, but still with no consideration of ductile detailing.

Throughout the 1990s, technical standards were updated with additional requirements and provisions. This period preceded the Eurocodes and saw the introduction of design using response spectrum analysis. This method is a linear elastic approach to calculate the modal, or peak, responses and was adopted for the design and sizing of the members. Construction features of this high seismic design (HSD) approach include frames in both directions, deformed rebars with higher yield strengths (430 MPa), concrete with higher compressive strength (25 MPa), but no mandatory capacity-based design and seismic detailing of members, as described in Gesualdi et al. [86].

The three construction practices described here have been labelled GLD (pre-1970s), SSD (1970–1980) and HSD (1980–2000). An online GitHub repository https://github.com/gerardjoreilly/Infilled-RC-Building-Database [87] has been created and will be further discussed below. It includes a more detailed overview of the design rules implemented for each of these three design periods for interested readers.

A2. Archetype design

This section describes the development of a database of archetype building models similar to Deierlein et al. [88] who benchmarked the seismic collapse performance of RC structures and Guan et al. [89] for special moment-resisting steel frame buildings in the US, for example. Based on expert architectural judgement, obtained through consultation with practitioners and review of past guidelines, the case study layouts were conceived, with examples illustrated in Fig. 15. The geometric configuration and architectural features were selected to reflect the function and form of the Italian design space over different building periods as much as possible. For instance, narrow hallways and corridors in dwellings generally 150 cm wide were an architectural feature of residential buildings constructed with infilled RC frames structures. Adjacent kitchens and bathrooms were also a common feature. Plumbing fixtures such as bathtubs, sinks and bidets whose dimensions were used for optimised space allocation were installed. Adequate separation of the day and night living spaces was an important feature. Windows with widths corresponding to a multiple of 45 or 60 cm were used. The staircase width did not exceed 3 m (i.e. wide enough to allow the passage of two people) and landings did not exceed a depth of 1.3 m. For perimeter walls corresponding to the façade of the building, a 24 cm infill was utilised, whereas for the separation of dwellings and encasing of stairs, a 30 cm infill of was used. Both considered thicknesses correspond to a double-leaf system used for thermal and acoustic insulation and fire-retarding. Considering walls used as interior partition elements for the compartmentalization of the living space within a single dwelling, a panel thickness of 80 mm is used corresponding to a single-leaf system. The architectural considerations highlighted herein do not just reflect the archetype design space adopted but can provide further information on the building's non-structural component inventory in an economic loss-oriented scenario, which is also an important facet in seismic risk assessment and classification.

Following the identification of key characteristics in terms of architectural features and design practice, a database of numerical models for infilled RC archetypes was developed. The database comprises 105 buildings corresponding to 7 plan layouts with 2-to-6 storeys each, for the three construction period designations previously described (i.e. GLD, SSD, HSD). As such, each single building was designated an index based on this. For

example, the index 2-C-SSD represents the 2-storey building with plan layout C designed following the SSD approach. Further details on their design are available in the online GitHub repository https://github.com/gerardjoreilly/Infilled-RC-Building-Database [87].

A3. Numerical modelling

Numerical models of the archetypes were developed in OpenSees [57] using a three-dimensional lumped plasticity approach. Beams and columns were modelled considering an elastic beam-column element with cracked section properties and zero-length elements located at a finite plastic hinge length, as illustrated in Figure 21. The empirical calibration for strength and deformation capacities and hysteresis parameters proposed by Di Domenico et al. [90] was adopted for columns with plain rebars (for GLD and SSD). The modelling approach by O'Reilly & Sullivan [67] was implemented considering an empirical calibration using experimental data. The flexural response of members was implemented in OpenSees through rotational springs (i.e. zero-length elements) and a *Pinching4* hysteretic material model. The shear strength model by Sezen and Moehle [91] was considered by coupling the flexural and shear springs in both principal directions at a finite plastic hinge location. For ductile members, which corresponds to the HSD cases, the flexural response parameters calibrated by Haselton et al. [92] were used and the shear response was modelled as elastic. Additionally, staircase elements were modelled to account for their added stiffness and potential to induce torsional behaviour, as implemented in O'Reilly et al. [93], for example.

For beam-column joints, the empirical relationships derived by De Risi et al. [94] and O'Reilly & Sullivan [67] were considered respectively for exterior and interior joints in non-ductile structures, with both approaches adopting a lumped scissors-type modelling approach. Joints with poor detailing and smooth reinforcing bars with end-hooks were modelled using zero-length elements using the *Hysteretic* material model in OpenSees to account for flexural and axial behaviours. Rigid offsets were accounted for adequately in the geometric dimensions of beam-column members. The modelling approach for beam-column joints is further illustrated in Figure 21.

Furthermore, the in-plane behaviour of masonry infill panels was modelled using the equivalent strut approach [95]. The option of single and double struts shown in Figure 21 is available in the models. The difference in infill strength (weak, medium and strong) used herein were considered following the characterization performed in Hak et al. [96]. Weak infills were used as internal partition elements within a single dwelling, whereas medium and strong infills were used for facades and partitioning of dwelling-to-dwelling and dwelling-to-stairway, as previously described.

These models have been fully implemented and are available at the aforementioned GitHub repository [87] along with several other useful documents and material regarding their structural behaviour and properties.

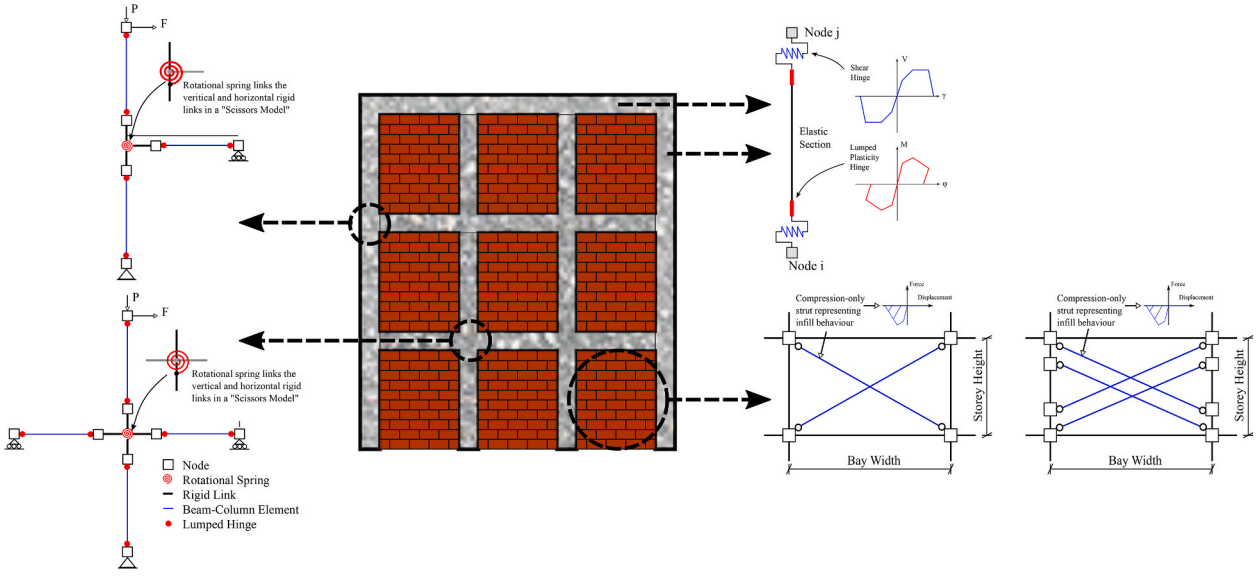

Fig. 21. Illustration of the numerical modelling approach used for the modelling of beam-column elements, interior and exterior beam-column joints and masonry infill panels for the archetype database of infilled RC building structures in OpenSees.

Al Mouayed Bellah Nafeh: Investigation, Methodology, Software, Data curation, Writing- Original draft preparation.

Gerard J. O'Reilly: Conceptualization, Investigation, Methodology, Supervision, Reviewing and Editing.

References

[1] European Standard. Eurocode 8: design of structures for earthquake resistance — Part 1: general rules, seismic actions and rules for buildings. European Committee for Standardization; 2003.

[2] Cs.Ll. Norme tecniche per le Costruzioni. *Decreto ministeriale, official gazette* 2008 (Ntc 2008). 2008. p. 1–89.

[3] De Luca F, Woods GED, Galasso C, D'Ayala D. RC infilled building performance against the evidence of the 2016 EEFIT Central Italy post-earthquake reconnaissance mission: empirical fragilities and comparison with the FAST method. Bull Earthq Eng 2018;16(7):2943–69. https://doi.org/10.1007/s10518-017-0289-1.

[4] Salvatore W, Caprilli S, Barberi V. Rapporto dei Danni Provocati dall'Evento Sismico del 6 Aprile sugli Edifici Scolastici del Centro Storico dell'Aquila. 2009.

[5] Del Gaudio C, De Martino G, Di Ludovico M, Manfredi G, Prota A, Ricci P, et al. Empirical fragility curves from damage data on RC buildings after the 2009 L'Aquila earthquake. Bull Earthq Eng 2017;15(4):1425–50. https://doi.org/10.1007/s10518-016-0026-1.

[6] Verderame GM, Iervolino I, Ricci P. Report on the damages on buildings following the seismic event of 6th of april 2009, V1.20. 2009.

[7] Cornell CA, Krawinkler H. Progress and challenges in seismic performance assessment. PEER Cent News 2000;3(2):1–4.

[8] Hazus FEMA. Earthquake model, technical manual. Federal Emergency Management Agency; 2003.

[9] Applied Technology Council. Seismic performance assessment of buildings. Fema P-58-5, vol. 1; 2018. December.

[10] Maio R, Tsionis G. Seismic fragility curves for the European building stock: review and evaluation of analytical fragility curves. 2016. https://doi.org/10.2788/586263.

[11] Gentile R, Galasso C. Simplicity versus accuracy trade-off in estimating seismic fragility of existing reinforced concrete buildings. Soil Dynam Earthq Eng 2021;144:106678. https://doi.org/10.1016/j.soildyn.2021.106678.

[12] Vamvatsikos D, Cornell CA. Direct estimation of seismic demand and capacity of multidegree-of-freedom systems through incremental dynamic analysis of single degree of freedom approximation. J Struct Eng 2005;131(4):589–99. https://doi.org/10.1061/(asce)0733-9445(2005)131:4(589).

[13] Baltzopoulos G, Baraschino R, Iervolino I, Vamvatsikos D. SPO2FRAG: software for seismic fragility assessment based on static pushover. Bull Earthq Eng 2017;15(10):4399–425. https://doi.org/10.1007/s10518-017-0145-3.

[14] Dolšek M, Fajfar P. Inelastic spectra for infilled reinforced concrete frames. Earthq Eng Struct Dynam 2004;33(15):1395–416. https://doi.org/10.1002/eqe.410.

[15] Dolšek M, Fajfar P. Simplified non-linear seismic analysis of infilled reinforced concrete frames. Earthq Eng Struct Dynam 2005;34(1):49–66. https://doi.org/10.1002/eqe.411.

[16] Guerrini G, Graziotti F, Penna A, Magenes G. Improved evaluation of inelastic displacement demands for short-period masonry structures. Earthq Eng Struct Dynam 2017;46(9):1411–30. https://doi.org/10.1002/eqe.2862.

[17] Gentile R, Galasso C. Surrogate probabilistic seismic demand modelling of inelastic single-degree-of-freedom systems for efficient earthquake risk applications. Earthq Eng Struct Dynam 2022;51(2):492–511. https://doi.org/10.1002/eqe.3576.

[18] Nettis A, Gentile R, Raffaele D, Uva G, Galasso C. Cloud Capacity Spectrum Method: accounting for record-to-record variability in fragility analysis using nonlinear static procedures. Soil Dynam Earthq Eng 2021;150:106829. https://doi.org/10.1016/j.soildyn.2021.106829.

[19] Freddi F, Padgett JE, Dall'Asta A. Probabilistic seismic demand modeling of local level response parameters of an RC frame. Bull Earthq Eng 2017;15(1):1–23. https://doi.org/10.1007/s10518-016-9948-x.

[20] O'Reilly GJ. Limitations of Sa(T 1) as an intensity measure when assessing non-ductile infilled RC frame structures. Bull Earthq Eng 2021;19(6):2389–417. https://doi.org/10.1007/s10518-021-01071-7.

[21] Nafeh AMB, O'Reilly GJ, Monteiro R. Simplified seismic assessment of infilled RC frame structures. Bull Earthq Eng 2020;18(4):1579–611. https://doi.org/10.1007/s10518-019-00758-2.

[22] Fema 274. NEHRP commentary on the guidelines for the seismic rehabilitation of buildings. Federal emergency management agency. Washington, DC: Developed by the Applied Technology Council; 1997 (October): 1–518.

[23] FEMA 440. Improvement of nonlinear static seismic analysis procedures. FEMA 440, vol. 440. Washington DC: Federal Emergency Management Agency; 2005. p. 392. June.

[24] Dávalos H, Miranda E. Evaluation of bias on the probability of collapse from amplitude scaling using spectral-shape-matched records. Earthq Eng Struct Dynam 2019;48(8):970–86. https://doi.org/10.1002/eqe.3172.

[25] Luco N, Bazzurro P. Does amplitude scaling of ground motion records result in biased nonlinear structural drift responses? Earthq Eng Struct Dynam 2007;36(13):1813–35. https://doi.org/10.1002/eqe.695.

[27] Heresi P, Miranda E. Intensity measures for regional seismic risk assessment of low-rise wood-frame residential construction. J Struct Eng 2021;147(1):04020287. https://doi.org/10.1061/(asce)st.1943-541x.0002859.

[28] O'Reilly GJ. Seismic intensity measures for risk assessment of bridges. Bull Earthq Eng 2021;19(9):3671–99. https://doi.org/10.1007/s10518-021-01114-z.

[29] Vamvatsikos D, Cornell CA. Applied incremental dynamic analysis. Earthq Spectra 2004;20(2):523–53. https://doi.org/10.1193/1.1737737.

[30] Jalayer F, Cornell CA. Alternative non-linear demand estimation methods for probability-based seismic assessments. Earthq Eng Struct Dynam 2009;38(8):951–72. https://doi.org/10.1002/eqe.876.

[31] Jalayer F, De Risi R, Manfredi G. Bayesian Cloud Analysis: efficient structural fragility assessment using linear regression. Bull Earthq Eng 2015;13(4):1183–203. https://doi.org/10.1007/s10518-014-9692-z.

[34] Watson-Lamprey J, Abrahamson N. Selection of ground motion time series and limits on scaling. Soil Dynam Earthq Eng 2006;26(5):477–82. https://doi.org/10.1016/j.soildyn.2005.07.001.

[36] Dávalos H, Miranda E. Evaluation of the scaling factor bias influence on the probability of collapse using SA(T1) as the intensity measure. Earthq Spectra 2019;35(2):679–702. https://doi.org/10.1193/011018EQS007M.

[37] Shome N, Cornell CA, Bazzurro P, Carballo JE. Earthquakes, records, and nonlinear responses. Earthq Spectra 1998;14(3):469–500. https://doi.org/10.1193/1.1586011.

[38] Coote-solek EW. Probabilistic seismic demand analysis of Nonlineer structures. 2004.

[39] Iervolino I, Cornell CA. Record selection for nonlinear seismic analysis of structures. Earthq Spectra 2005;21(3):685–713. https://doi.org/10.1193/1.1990199.

[40] Bazzurro P, Luco N. Do scaled and spectrum-matched near-source records produce biased nonlinear structural responses?. In: 8th US National Conference on earthquake engineering 2006, vol. 15; 2006. San Francisco, CA.

[41] Baker JW. Measuring bias in structural response caused by ground motion scaling. Pacific Conf Earthq Eng 2007;56:1–6. https://doi.org/10.1002/eqe.

[42] Zacharenaki A, Fragiadakis M, Assimaki D, Papadrakakis M. Bias assessment in Incremental Dynamic Analysis due to record scaling. Soil Dynam Earthq Eng 2014;67:158–68. https://doi.org/10.1016/j.soildyn.2014.09.007.

[43] Dávalos H, Miranda E. Filtered incremental velocity: a novel approach in intensity measures for seismic collapse estimation. Earthq Eng Struct Dynam 2019;48(12):1384–405. https://doi.org/10.1002/eqe.3205.

[44] Eads L, Miranda E, Lignos DG. Average spectral acceleration as an intensity measure for collapse risk assessment. Earthq Eng Struct Dynam 2015;44(12):2057–73. https://doi.org/10.1002/eqe.2575.

[45] Rota M, Penna A, Strobbia CL. Processing Italian damage data to derive typological fragility curves. Soil Dynam Earthq Eng 2008;28(10–11):933–47. https://doi.org/10.1016/j.soildyn.2007.10.010.

[46] Akkar S, Sucuoğlu H, Yakut A. Displacement-based fragility functions for low- and mid-rise ordinary concrete buildings. Earthq Spectra 2005;21(4):901–27. https://doi.org/10.1193/1.2084232.

[47] Erberik MA. Fragility-based assessment of typical mid-rise and low-rise RC buildings in Turkey. Eng Struct 2008;30(5):1360–74. https://doi.org/10.1016/j.engstruct.2007.07.016.

[48] Rossetto T, Elnashai A. Derivation of vulnerability functions for European-type RC structures based on observational data. Eng Struct 2003;25(10):1241–63. https://doi.org/10.1016/S0141-0296(03)00060-9.

[49] Kohrangi M, Bazzurro P, Vamvatsikos D, Spillatura A. Conditional spectrum-based ground motion record selection using average spectral acceleration. Earthq Eng Struct Dynam 2017;46(10):1667–85. https://doi.org/10.1002/eqe.2876.

[50] Vamvatsikos D, Bakalis K, Kohrangi M, Pyrza S, Castiglioni CA, Kanyilmaz A, et al. A risk-consistent approach to determine EN1998 behaviour factors for lateral load resisting systems. Soil Dynam Earthq Eng 2020:131. https://doi.org/10.1016/j.soildyn.2019.106008. May 2018.

[53] Jalayer F, Ebrahimian H, Miano A, Manfredi G, Sezen H. Analytical fragility assessment using unscaled ground motion records. Earthq Eng Struct Dynam 2017;46(15):2639–63. https://doi.org/10.1002/eqe.2922.

[55] Vamvatsikos D, Cornell CA. Direct estimation of the seismic demand and capacity of oscillators with multi-linear static pushovers through IDA. Earthq Eng Struct Dynam 2006;35(9):1097–117. https://doi.org/10.1002/eqe.573.

[56] Vidic T, Fajfar P, Fischinger M. Consistent inelastic design spectra: strength and displacement. Earthq Eng Struct Dynam 1994;23(5):507–21. https://doi.org/10.1002/eqe.4290230504.

[57] McKenna F. OpenSees: a framework for earthquake engineering simulation. Comput Sci Eng 2011;13(4):58–66. https://doi.org/10.1109/MCSE.2011.66.

[58] Eads L, Miranda E, Lignos D. Spectral shape metrics and structural collapse potential. Earthq Eng Struct Dynam 2016;45. https://doi.org/10.1002/eqe.2739.

[59] Esteghamati MZ, Huang Q. An efficient stratified-based ground motion selection for cloud analysis. In: 13th International Conference on applications of statistics and probability in civil engineering. Seoul, South Korea: ICASP 2019; 2019. https://doi.org/10.22725/ICASP13.399.

[60] O'Reilly GJ, Kohrangi M, Bazzurro P, Monteiro R. Intensity measures for the collapse assessment of infilled RC frames. In: 16th European Conference on earthquake engineering, Thessaloniki; 2018.

[61] O'Reilly GJ, Monteiro R. Probabilistic models for structures with bilinear demand-intensity relationships. Earthq Eng Struct Dynam 2019;48(2):253–68. https://doi.org/10.1002/eqe.3135.

[62] O'Reilly GJ, Nafeh AMB. Infilled-RC-building-response-estimation. GitHub Reposit 2021. https://doi.org/10.5281/zenodo.5082996.

[63] Pagani M, Monelli D, Weatherill G, Danciu L, Crowley H, Silva V, et al. Openquake engine: an open hazard (and risk) software for the global earthquake model. Seismol Res Lett 2014;85(3):692–702. https://doi.org/10.1785/0220130087.

[64] Mori F, Mendicelli A, Moscatelli M, Romagnoli G, Peronace E, Naso G. A new Vs30 map for Italy based on the seismic microzonation dataset. Eng Geol 2020;275:105745. https://doi.org/10.1016/j.enggeo.2020.105745.

[65] Verdi VI a G, Cb AC, Famiglia FDI, Popolazione D, Abitazioni ED. Censimento generale della popolazione e delle abitazioni, vols. 1–24; 2011.

[66] Crowley H, Despotaki V, Rodrigues D, Silva V, Toma-Danila D, Riga E, et al. Exposure model for European seismic risk assessment. Earthq Spectra 2020;36(1_suppl):252–73. https://doi.org/10.1177/8755293020919429.

[67] O'Reilly GJ, Sullivan TJ. Modeling techniques for the seismic assessment of the existing Italian RC frame structures. J Earthq Eng 2019;23(8):1262–96. https://doi.org/10.1080/13632469.2017.1360224.

[68] O'Reilly GJ, Sullivan TJ. Probabilistic seismic assessment and retrofit considerations for Italian RC frame buildings. Bull Earthq Eng 2018;16(3):1447–85. https://doi.org/10.1007/s10518-017-0257-9.

[69] Fardis MN, Calvi GM. Effects of infills on the global response of reinforced concrete frames. In: Proceedings on the 10th European Conference on earthquake engineering, Vienna. Rotterdam: Balkema; 1994.

[70] Dolšek M, Fajfar P. The effect of masonry infills on the seismic response of a four-storey reinforced concrete frame - a deterministic assessment. Eng Struct 2008;30(7):1991–2001. https://doi.org/10.1016/j.engstruct.2008.01.001.

[71] Dolšek M, Fajfar P. The effect of masonry infills on the seismic response of a four storey reinforced concrete frame-a probabilistic assessment. Eng Struct 2008;30(11):3186–92. https://doi.org/10.1016/j.engstruct.2008.04.031.

[72] Dolek M, Fajfar P. Mathematical modelling of an infilled RC frame structure based on the results of pseudo-dynamic tests. Earthq Eng Struct Dynam 2002;31(6):1215–30. https://doi.org/10.1002/eqe.154.

[73] Lu J, Elgamal A, Mackie K, Shamsabadi A. A framework for performance-based earthquake engineering of bridge-abutment systems. In: Proceedings of the 2003 Pacific Conference on earthquake engineering; 2012. p. 1680–9. https://doi.org/10.1061/9780784412121.173.

[74] ATC. Quantification. Of building seismic performance factors. 2009.

[75] Perrone D, Brunesi E, Filiatrault A, Nascimbene R. Probabilistic estimation of floor response spectra in masonry infilled reinforced concrete building portfolio. Eng Struct 2020;202(March 2019):109842. https://doi.org/10.1016/j.engstruct.2019.109842.

[76] R.D.. Norme per l'esecuzione di opere in conglomerato cementizio semplice o armato - R.D. 16.11.1939 n°2229. 1939.

[77] Pagano M. Teoria degli edifici vol. II Edifici in cemento armato. Edizione L. 1977.

[78] Santarella L. Il cemento armato vol.2: le applicazioni alle costruzioni civili e industriali, vol. 2. Edizione H; 1957. in Italian.
[79] Crowley H, Despotaki V, Silva V, Dabbeek J, Romão X, Pereira N, et al. Model of seismic design lateral force levels for the existing reinforced concrete European building stock. Bull Earthq Eng 2021;19(7):2839–65. https://doi.org/10.1007/s10518-021-01083-3.
[80] Fajfar P. Analysis in seismic provisions for buildings: past, present and future. Geotechn, Geol Earthq Eng 2018;46. https://doi.org/10.1007/978-3-319-75741-4_1.
[81] Crowley H, Rodrigues D, Silva V, Despotaki V, Martins L, Romão X, et al. The European Seismic Risk Model 2020 (ESRM 2020). In: ICONHIC 2019 2nd International Conference on Natural Hazards & Infrastructure; 2019. p. 1–12. 2020 (June 2019).
[82] Romão X, Pereira N, Castro M, De Maio F, Crowley H, Silva V, et al. European building vulnerability database v1.0. 2020.
[83] Precettive D. Legge 5 Novembre 1971 n . 1086 Norme per la disciplina delle opere di conglomerato cementizio armato , normale e precompresso ed a struttura metallica. 1971.
[84] D.M.LL.PP 16/01/96. Norme Tecniche per le costruzioni in zone sismiche. 1994.
[85] Decreto Ministeriale. Norme tecniche relative alle costruzioni antisismiche. 1986. D.M. 108/1986 (in Italian).
[86] Gesualdi G, Viggiani LRS, Cardone D. Seismic performance of RC frame buildings accounting for the out-of-plane behavior of masonry infills. Bull Earthq Eng 2020;18(11):5343–81. https://doi.org/10.1007/s10518-020-00904-1.
[87] O'Reilly GJ, Nafeh AMB. Infilled-RC-building-database. GitHub Reposit 2021. https://doi.org/10.5281/zenodo.5082990.
[88] Deierlein GG, Liel AB, Haselton CB, Kircher CA. ATC 63 methodology for evaluating seismic collapse safety of archetype buildings. In: Proceedings of the 2008 structures Congress - structures Congress 2008: Crossing the borders, vol. 314; 2008. https://doi.org/10.1061/41016(314)48.
[89] Guan M, Eeri X, Burton M, Eeri H, Shokrabadi M. A database of seismic designs, nonlinear models, and seismic responses for steel moment-resisting frame buildings. Earthq Spectra 2021;37(2):1199–222. https://doi.org/10.1177/8755293020971209.
[90] Di Domenico M, Ricci P, Verderame GM. Empirical calibration of hysteretic parameters for modelling the seismic response of reinforced concrete columns with plain bars. Eng Struct 2021;237:112120. https://doi.org/10.1016/j.engstruct.2021.112120.
[91] Sezen H, Moehle JP. Shear strength model for lightly reinforced concrete columns. J Struct Eng 2004;130(11):1692–703. https://doi.org/10.1061/(asce)0733-9445(2004)130:11(1692).
[92] Haselton CB, Liel AB, Lange ST. Beam-column element model calibrated for predicting flexural response leading to global collapse of RC frame buildings. PeerJ 2008;3(May). 2007.
[93] O'Reilly GJ, Perrone D, Fox M, Monteiro R, Filiatrault A, Lanese I, et al. System identification and seismic assessment modeling implications for Italian school buildings. J Perform Constr Facil 2019;33(1):04018089. https://doi.org/10.1061/(asce)cf.1943-5509.0001237.
[94] De Risi MT, Ricci P, Verderame GM. Modelling exterior unreinforced beam-column joints in seismic analysis of non-ductile RC frames. Earthq Eng Struct Dynam 2017;46(6):899–923. https://doi.org/10.1002/eqe.2835.
[95] Crisafulli FJ, Carr AJ, Park R. Analytical modelling of infilled frame structures - a general review. Bull N Z Soc Earthq Eng 2000;33(1):30–47. https://doi.org/10.5459/bnzsee.33.1.30-47.
[96] Hak S, Morandi P, Magenes G, Sullivan TJ. Damage control for clay masonry infills in the design of RC frame structures. J Earthq Eng 2012;16(SUPPL. 1):1–35. https://doi.org/10.1080/13632469.2012.670575.